NJC

PAPER

View Article Online
View Journal | View Issue

Cite this: *New J. Chem.*, 2018, 42, 18667

High-spin enforcement in first-row metal complexes of a constrained polyaromatic ligand: synthesis, structure, and properties†

Lizhu Chen,[a] Hunter A. Dulaney,[a] Branford O. Wilkins,[b] Sarah Farmer,[a] Yanbing Zhang,[a] Frank R. Fronczek[c] and Jonah W. Jurss*[a]

Received 27th April 2018,
Accepted 19th October 2018

DOI: 10.1039/c8nj02072h

rsc.li/njc

The coordination chemistry of a rigid tetradentate polypyridyl ligand has been developed with first-row transition metals Mn(II), Fe(II), Co(II), Ni(II), and Zn(II). The polyaromatic ligand, 2,2′-di([2,2′-bipyridin]-6-yl)-1,1′-biphenyl (**5**, bpbb), is comprised of 2,2′-bipyridine donors positioned at the 2 and 2′ carbons of a biphenyl backbone. Notably, coordination of the typical strong field bipyridine fragments is constrained, weakening the octahedral ligand fields around manganese, iron, and cobalt to give high-spin electronic states. Solution magnetic susceptibility measurements were conducted across the series using the Evans method and variable-temperature solid-state SQUID magnetometry was performed on two Fe(II) compounds, including a bis(thiocyanato) species. Spin crossover behavior was not observed as the compounds remained high-spin over the entire temperature range. The impact of the biphenyl bridge on M–N bond distances and redox potentials has also been assessed by comparison to relevant first-row metal bis- and tris-bipyridine compounds from the literature.

Introduction

Tetradentate and pentadentate ligand frameworks are important classes of ligands for accessing stable first-row transition metal complexes. The metal–ligand bonds of 3d metals are often labile and prone to substitution. Thus, highly chelating ligands are frequently employed to counter this characteristic while affording well-defined coordination spheres with tunable properties. Given the high denticity of these ligand classes, the number and relative orientation of labile coordination sites can be controlled, and specific geometries enforced, by clever ligand design in which preorganization, rigidity, and steric factors are useful strategies.[1,2]

Biphenyl-based polydentate ligands have been employed in a number of areas, including bioinorganic model compounds,[2–4] spin crossover complexes,[5] and homogeneous catalysis.[6] These systems exploit biphenyl as an unyielding structural unit whose substituted phenyl groups are not coplanar, allowing the appended donors to bind at a single metal center but with limited flexibility. Octahedral Fe(II) compounds of general form $[FeL_6]^{2+}$ or $FeL_4(NCS)_2$ (where L is an N-heterocyclic donor such as pyridine) comprise the vast majority of known spin crossover (SCO) compounds, which hold great promise for applications such as data storage and molecular electronics.[7–9] SCO compounds are typically studied in the solid state where abrupt transitions between spin states can be observed.[7–9] One strategy used to engender SCO behavior is the design of sterically demanding ligands that allow tuning of the metal–ligand bonding interactions to access complexes in which the ligand field strength and the spin-pairing energy are comparable.[10,11] This commonly manifests through added substituents at positions adjacent to the donor atoms (*i.e.* the 6 and 6′ positions of 2,2′-bipyridine or the 2 and 9 positions of 1,10-phenanthroline).[12,13]

In this context, we sought to introduce strain remotely using a rigid polydentate scaffold as an underexplored approach to SCO compounds. Our laboratory has been interested in preorganized frameworks,[14] as in the present case which involves a tetradentate ligand that maximizes the chelate effect while dictating the metal coordination geometry through limited rotation about single bonds connecting rigid donor moieties. Herein we report a straightforward and improved synthesis of polyaromatic ligand 2,2′-di([2,2′-bipyridin]-6-yl)-1,1′-biphenyl[2] and its metalation with mid-to-late first-row transition metals. Metal complexes of Mn(II), Fe(II), Co(II), Ni(II), and Zn(II) were prepared to evaluate how the structural constraints of the ligand are balanced with the geometric and electronic preferences of

[a] *Department of Chemistry and Biochemistry, University of Mississippi, University, MS 38677, USA. E-mail: jwjurss@olemiss.edu*
[b] *Department of Chemistry, Texas A&M University, College Station, TX 77843, USA*
[c] *Department of Chemistry, Louisiana State University, Baton Rouge, LA 70803, USA*

† Electronic supplementary information (ESI) available. CCDC 1837621 (**5-Mn**), 1837622 (**5-Fe**), 1837623 (**5-Co**), 1837624 (**5-Ni**), and 1837625 (**5-Zn**). For ESI and crystallographic data in CIF or other electronic format see DOI: 10.1039/c8nj02072h

the metal centers. Solid-state structures and optical, magnetic, and electrochemical properties of this series are described.

Experimental section

Materials and methods

Unless otherwise noted, all synthetic manipulations were carried out using standard Schlenk techniques or in an MBraun glovebox under nitrogen atmosphere. Tetrahydrofuran, dichloromethane, toluene, and diethyl ether were dried with a Pure Process Technology solvent purification system. Compounds iodomethane, phosphorus(v) oxybromide, 2-tri-*n*-butylstannylpyridine, chlorobenzene, palladium(0) tetrakis(triphenylphosphine), and dichloro(*p*-cymene)ruthenium(II) dimer were purchased from Oakwood Chemicals. Anhydrous metal salts, iron(II) trifluoromethanesulfonate and iron(III) chloride, were purchased from Strem Chemicals and Fisher Scientific, respectively. Potassium hexacyanoferrate(III) was purchased from Sigma Aldrich and 2-phenylpyridine was acquired from Chem-Impex International. Water was purified with a Barnstead NANOpure Diamond system. All other chemicals were reagent or ACS grade, purchased from commercial vendors, and used without further purification. ^{1}H and ^{13}C NMR spectra were obtained using Bruker spectrometers operating at 500 MHz (^{1}H) or 126 MHz (^{13}C) as noted. Spectra were calibrated to residual protiated solvent peaks; chemical shifts are reported in ppm. High-resolution electrospray ionization mass spectra (HR-ESI-MS) were obtained with a Waters SYNAPT HDMS Q-TOF mass spectrometer and elemental analyses of carbon, hydrogen, and nitrogen were conducted by Atlantic Microlab, Inc., Norcross, Georgia. UV-Vis spectra were recorded on an Agilent/Hewlett-Packard 8453 UV-Visible Spectrophotometer with diode-array detector. Solution magnetic susceptibilities were determined by NMR using the Evans method.[15]

Electrochemical measurements

Electrochemistry was performed with a Bioanalytical Systems, Inc. (BASi) Epsilon potentiostat employing a three-electrode cell equipped with glassy carbon disk (3 mm dia.) working electrode, platinum wire counter electrode, and a silver wire quasi-reference electrode. Cyclic voltammograms were collected in anhydrous acetonitrile containing 0.1 M Bu_4NPF_6 electrolyte, and referenced at the end of experiments using ferrocene as an internal standard.

X-ray crystallography

Single crystals were coated with Paratone-N hydrocarbon oil and mounted on the tip of a MiTeGen micromount. Temperature was maintained at 100 K with an Oxford Cryostream 700 during data collection at the University of Mississippi, Department of Chemistry and Biochemistry, X-ray Crystallography Facility. Samples were irradiated with Mo-Kα radiation with λ = 0.71073 Å using a Bruker Smart APEX II diffractometer equipped with a Microfocus Sealed Source (Incoatec IμS) and APEX-II detector. The Bruker APEX2 v. 2009.1 software package was used to integrate raw data which were corrected for Lorentz and polarization effects.[16] A semi-empirical absorption correction (SADABS) was applied.[17] Space groups were identified based on systematic absences, E-statistics, and successive refinement of the structures. The structures were solved using direct methods and refined by least-squares refinement on F^2 and standard difference Fourier techniques using SHELXL.[18] Thermal parameters for all non-hydrogen atoms were refined anisotropically, and hydrogen atoms were included at ideal positions. For the structure of **5-Zn**, a poorly resolved outer-sphere diethyl ether molecule could not be successfully modeled in the difference map. The data was treated with the SQUEEZE procedure in PLATON.[19] Full details of the structure determination in CIF format have been deposited into The Cambridge Crystallographic Data Centre (CCDC), and have the following deposition numbers: CCDC 1837621 (**5-Mn**), 1837622 (**5-Fe**), 1837623 (**5-Co**), 1837624 (**5-Ni**), and 1837625 (**5-Zn**).† Coordination polyhedra for the central metal atoms were produced using the Diamond 4.0 Crystal and Molecular Structure Visualization program.[20]

SQUID magnetometry

For both iron-containing compounds, crystals were crushed into a polycrystalline powder and loaded into NORELL quartz NMR tubes. A slight excess by mass of eicosane was deposited on top of the powder and the quartz tubes were flame sealed under vacuum. The eicosane was melted in a warm water bath (42 °C) and allowed to re-solidify in order to immobilize the powder samples. The sealed tubes were placed in straw sample holders, and these sample holders were loaded into a Quantum Design MPMS 3 SQUID magnetometer (TAMU Vice President of Research). DC (direct current) magnetic susceptibility measurements of the samples were recorded under a static magnetic field of 0.1 T in the temperature range of 300 K to 2 K. The data was corrected for diamagnetic contributions from the straw and the quartz tube. The intrinsic diamagnetism of the iron complexes and eicosane was also corrected for by using Pascal's constants.[15]

Synthesis

A literature procedure was used for the preparation of 2,2′-di(pyridin-2-yl)-1,1′-biphenyl, precursor **1**.[21] A different synthetic route to ligand **5** (bpbb) has been reported previously.[2]

2,2′-([1,1′-Biphenyl]-2,2′-diyl)bis(1-methylpyridin-1-ium) iodide, 2. To a solution of **1** (0.50 g, 1.6 mmol) in acetonitrile (10 mL), iodomethane (1.5 mL, 24.1 mmol) was added dropwise under nitrogen and the solution was refluxed for 2 days. A yellow suspension forms over the course of the reaction. The reaction mixture is allowed to cool to room temperature before diethyl ether (25 mL) is added and the precipitate is collected by vacuum filtration, washed with diethyl ether, and dried to yield a light yellow solid (1.05 g, 60%). ^{1}H NMR (MeOD, 500 MHz): δ 9.13 (d, J = 6.3 Hz, 2H), 8.41 (t, J = 7.9 Hz, 2H), 8.07 (t, J = 1.6 Hz, 2H), 7.8 (dd, J = 8.0, 7.6 Hz, 4H), 7.62 (t, J = 7.6, 2H), 7.56–7.49 (bt, 2H), 7.12 (s, 2H). ^{13}C NMR (MeOD, 126 MHz): δ 148.878 (s), 146.75 (s), 138.81 (s), 133.60 (s), 133.03 (s), 132.56 (s), 132.17 (s), 131.84 (s), 130.86 (s), 130.35 (s), 128.82 (s), 128.37 (s). HR-ESI-MS (M^+) m/z calc. for $[2]^{2+}$, 169.0891, found, 169.0901.

6,6′-([1,1′-Biphenyl]-2,2′-diyl)bis(1-methylpyridin-2(1*H*)-one), 3. This reaction is performed under air. $K_3Fe(CN)_6$ (2.48 g, 7.54 mmol) was dissolved in water (10.3 mL) and cooled to 0 °C. Next, NaOH (2.51 g, 62.8 mmol) in water (9.4 mL) and **2** (0.93 g, 1.57 mmol) in water (4.7 mL) were added dropwise to the first solution, simultaneously, *via* two dropping funnels over a period of 1.5 h. The reaction mixture was then stirred for 3 h at 0 °C before it was heated at 40 °C overnight. Saturated aqueous NaCl (28 mL) was added before dichloromethane (3 × 50 mL) was used to extract the product. The organic phase was dried over anhydrous Na_2SO_4 and taken to dryness by rotary evaporation. The resulting solid was dissolved in 8 : 2 ethyl acetate : methanol, filtered through neutral alumina to remove impurities and taken to dryness. Finally, the solid was dissolved in a minimum amount of dichloromethane to which hexanes was added to produce a light yellow solid that was collected by vacuum filtration to yield product (0.33 g, 76%). ^{1}H NMR ($CDCl_3$, 500 MHz): δ 7.51 (dt, J = 1.4 Hz, J = 7.5 Hz, 2H), 7.44 (dd, J = 1.4 Hz, J = 7.5 Hz, 2H), 7.39 (dd, J = 1.5 Hz, J = 7.4 Hz, 2H), 7.20 (dd, J = 1.4 Hz, J = 7.6 Hz, 2H), 7.12 (t, J = 7.15 Hz, 2H), 6.48 (dd, J = 1.4 Hz, J = 9.2 Hz, 2H), 5.45 (d, J = 6.9 Hz, 2H), 3.0 (s, 6H). ^{13}C NMR ($CDCl_3$, 126 MHz): δ 139.59 (s), 138.44 (s), 133.70 (s), 132.26 (s), 130.48 (s), 129.88 (s), 129.62 (s), 128.45 (s), 128.31 (s), 118.90 (s), 118.79 (s), 34.59 (s). HR-ESI-MS (M^+) m/z calc. for [**3** + Cs^+], 501.0579, found, 501.0574.

2,2′-Bis(6-bromopyridin-2-yl)-1,1′-biphenyl, 4. In an oven-dried flask, 10 equivalents of phosphorus(v) oxybromide (1.95 g, 6.8 mmol) was added to **3** (0.25 g, 0.68 mmol) and heated to 105 °C overnight with stirring under nitrogen atmosphere. The reaction was allowed to cool to room temperature and quenched with aqueous NH_4OH until strongly basic. The resulting precipitate was collected by filtration and washed with water. Dichloromethane was used to dissolve the solid before it was washed three times with water in a separatory funnel. The organic phase was dried over anhydrous sodium sulfate and evaporated to dryness to afford a light yellow solid, which was purified by silica gel column chromatography eluting with 15 : 1 hexanes : ethyl acetate to yield a pure white solid (0.29 g, 92%). ^{1}H NMR ($CDCl_3$, 500 MHz): δ 7.53 (m, 2H), 7.49–7.44 (m, 2H), 7.45–7.39 (m, 4H), 7.27 (dd, J = 0.9 Hz, J = 7.8 Hz, 2H), 7.20 (t, J = 7.7 Hz, 2H), 6.68 (dd, J = 0.85 Hz, J = 7.6, 0.9 Hz, 2H). ^{13}C NMR ($CDCl_3$, 126 MHz): δ 158.70 (s), 141.59 (s), 139.54 (s), 138.47 (s), 137.83 (s), 131.29 (s), 130.41 (s), 129.39 (s), 128.28 (s), 125.87 (s), 123.34 (s). HR-ESI-MS (M^+) m/z calc. for [**4** + Cs^+], 596.8578, found, 596.8571.

2,2′-Di([2,2′-bipyridin]-6-yl)-1,1′-biphenyl, 5 (bpbb). In an oven-dried flask, **4** (0.25 g, 0.50 mmol) was dissolved in anhydrous toluene to which a solution of 2-tributylstannylpyridine (0.49 g, 1.33 mmol) in anhydrous toluene was added dropwise. Then, 0.8 mol % of $Pd(PPh_3)_4$ (4.9 mg, 0.004 mmol) was added and the reaction mixture was refluxed for 72 hours. After it was cooled to room temperature, the solvent was removed, and purification was achieved by silica gel column chromatography eluting with 1 : 1 : 0.1 ethyl acetate : hexanes : dichloromethane to yield a white solid (0.143 g, 82%). ^{1}H NMR (500 MHz, $CDCl_3$): δ 8.58 (d, J = 4.8 Hz, 1H), 8.06 (d, J = 7.8 Hz, 1H), 7.65–7.57 (m, 2H), 7.53 (d, J = 7.4 Hz, 2H), 7.47 (t, J = 7.2 Hz, 1H), 7.43–7.24 (m, 2H), 7.25–7.20 (m, 1H), 6.84 (d, J = 7.8 Hz, 1H). ^{13}C NMR spectra matched previously reported data.[2] HR-ESI-MS (M^+) m/z calc. for [**5** + H^+], 463.1923, found, 463.1917.

***5-Mn**, [Mn(bpbb)(OH$_2$)(OTf)][OTf].* In a round bottom flask, $[Mn(MeCN)_2(OTf)_2]_n$ (47 mg, 0.11 mmol) and **5** (50 mg, 0.11 mmol) were added and subsequently dissolved in acetonitrile. After stirring under nitrogen at room temperature overnight, the reaction mixture was taken to dryness by rotary evaporation. The manganese complex was recrystallized from acetonitrile with slow diethyl ether diffusion. Crystals were collected, dried under vacuum, and exposed to air to give the compound as indicated. Yield = 94 mg (90%). Elem. anal. calc. for $C_{34}H_{24}F_6MnN_4O_7S_2$: C, 48.99; H, 2.90; N, 6.72. Found: C, 49.08; H, 3.01; N, 6.67. HR-ESI-MS (M^+) m/z calc. for $[Mn(bpbb)(OTf)]^+$, 666.0745, found, 666.0731.

***5-Fe**, [Fe(bpbb)(MeCN)(OTf)][OTf].* In a round bottom flask, $Fe(OTf)_2$ (0.11 g, 3.1 mmol) and **5** (0.14 g, 3.1 mmol) were added and subsequently dissolved in methanol. The mixture was stirred under nitrogen at room temperature overnight. The solvent was subsequently removed by rotary evaporation, and the solid was re-dissolved in acetonitrile. Crystals were obtained by slow diffusion of diethyl ether into the concentrated solution. Yield = 93 mg (89%). Elem. anal. calc. for $C_{36}H_{25}F_6FeN_5O_6S_2\cdot(H_2O)_{1.5}\cdot(C_4H_{10}O)_{0.5}$: C, 49.52; H, 3.61; N, 7.60. Found: C, 49.27; H, 3.57; N, 7.20. HR-ESI-MS (M^+) m/z calc. for $[Fe(bpbb)(OTf)]^+$, 667.0715, found, 667.0717.

***5-Co**, [Co(bpbb)(MeCN)(OTf)][OTf].* In a round bottom flask, $Co(MeCN)_2(OTf)_2$ (48 mg, 0.11 mmol) and **5** (50 mg, 0.11 mmol) were added and subsequently dissolved in acetonitrile. After stirring under nitrogen at room temperature overnight, the pink orange reaction mixture was concentrated. Crystals of the cobalt complex were obtained by slow diethyl ether diffusion into the solution, collected, dried under vacuum. Yield = 95 mg (90%). Elem. anal. calc. for $C_{36}H_{25}CoF_6N_5O_6S_2\cdot(H_2O)_{1.5}\cdot(C_4H_{10}O)_{0.5}$: C, 49.36; H, 3.60; N, 7.57. Found: C, 49.14; H, 3.49; N, 7.23. HR-ESI-MS (M^+) m/z calc. for $[Co(bpbb)(OTf)]^+$, 670.0696, found, 670.0615.

***5-Ni**, [Ni(bpbb)(MeCN)(ClO$_4$)](ClO$_4$).* **Caution**! Perchlorate salts are potentially explosive and should be handled in small amounts with care! In a round bottom flask, $Ni(ClO_4)_2\cdot 6H_2O$ (40 mg, 0.11 mmol) and **5** (50 mg, 0.11 mmol) were added and subsequently dissolved in acetonitrile (10 mL). After stirring under nitrogen at room temperature overnight, the light violet reaction mixture was taken to dryness by rotary evaporation. Crystals of the resulting nickel complex were grown from acetonitrile with slow diethyl ether diffusion. Yield = 84 mg (91%). Elem. anal. calc. for $C_{34}H_{25}Cl_2N_5NiO_8\cdot(H_2O)_{0.5}\cdot(MeCN)_{0.5}$: C, 53.16; H, 3.51; N, 9.74. Found: C, 53.12; H, 3.50; N, 9.76. HR-ESI-MS (M^+) m/z calc. for $[Ni(bpbb)(ClO_4)]^+$, 619.0683, found, 619.0670.

***5-Zn**, [Zn(bpbb)(OTf)][OTf].* In a round bottom flask, $Zn(OTf)_2$ (39 mg, 0.11 mmol) and **5** (50 mg, 0.11 mmol) were added and subsequently dissolved in acetonitrile. After stirring under nitrogen at room temperature overnight, the colorless reaction mixture was taken to dryness by rotary evaporation. Crystals of

the resulting zinc complex were grown from acetonitrile with slow diethyl ether diffusion. Yield = 91 mg (90%). ^{1}H NMR (CD_3CN, 500 MHz): δ 8.47 (m, 3H), 8.29 (dt, J = 1.65, 7.9 Hz, 1H), 8.22 (dd, J = 1.3, 5 Hz, 1H), 8.10 (dd, J = 2.45, 6.5 Hz, 1H), 7.65 (dt, J = 1.01, 5.4 Hz, 1H), 7.50 (d, J = 7.6 Hz, 1H), 7.31 (t, J = 7.5 Hz, 1H), 7.24 (dt, J = 0.8, 8.4 Hz, 1H), 6.91 (d, J = 7.65 Hz, 1H). Elem. Anal. calc. for $C_{34}H_{22}F_6N_4O_6S_2Zn$: C, 49.44; H, 2.68; N, 6.78. Found: C, 49.71; H, 2.81; N, 6.73. HR-ESI-MS (M^+) m/z calc. for $[Zn(bpbb)]^+$, 675.0656, found 675.0629.

5-Fe(NCS)$_2$, *Fe(bpbb)(NCS)$_2$.* In a round bottom flask, $FeSO_4 \cdot 7H_2O$ (50 mg, 0.18 mmol) and NaSCN (29 mg, 0.39 mmol) were added in methanol. The mixture was stirred under nitrogen at room temperature. The mixture immediately formed a white precipitate. The mixture was filtered through Celite. Ligand **5** (83 mg, 0.18 mmol) was added to the colorless filtrate which turned purple immediately and was stirred overnight under nitrogen. The solvent was then removed by rotary evaporation. The resulting solid was dissolved in acetonitrile, and crystals were obtained by slow diffusion of diethyl ether into the concentrated solution. Yield = 108 mg (95%). Elem. anal. calc. for $C_{34}H_{22}FeN_6S_2$: C, 64.36; H, 3.49; N, 13.24. Found: C, 64.62; H, 3.64; N, 13.05. HR-ESI-MS (M^+) m/z calc. for $[Fe(bpbb)(NCS)]^+$, 576.0946, found, 576.0925.

Synthesis

The seminal publication involving ligand **5** reported a synthesis (Fig. 1A) with an overall yield of just 18%.[2] We have established an improved route to this compound as shown in Fig. 1B. Briefly, a ruthenium-catalyzed homocoupling of 2-phenylpyridine affords precursor **1**.[21] Next, procedures for 2,2′-bipyridine functionalization were adapted,[22] beginning with the methylation of **1** to form intermediate **2** as a light yellow precipitate that is simply collected by filtration. Oxidation of **2** with potassium ferricyanide gives **3** in high yield, followed by bromination with phosphorus oxytribromide to produce **4**. Notably, compound **4** is a versatile intermediate for future substitution of electronically disparate donor moieties for ligand tunability. A palladium-catalyzed Stille coupling with 2-(tributylstannyl)pyridine gives the desired bipyridine-derivatized product **5** in 30% overall yield. We note that methylation of **1** gives a mixture of mono- and dimethylated (**2**) products. In practice, the product mixture is carried through the next two steps and undesired compounds are removed during purification of **4**, which was found to be easiest.

Complexation of metal ions Mn(II), Fe(II), Co(II), Ni(II), and Zn(II) was performed in acetonitrile or methanol solutions by stirring **5** with the appropriate metal precursor in a 1 : 1 ratio at

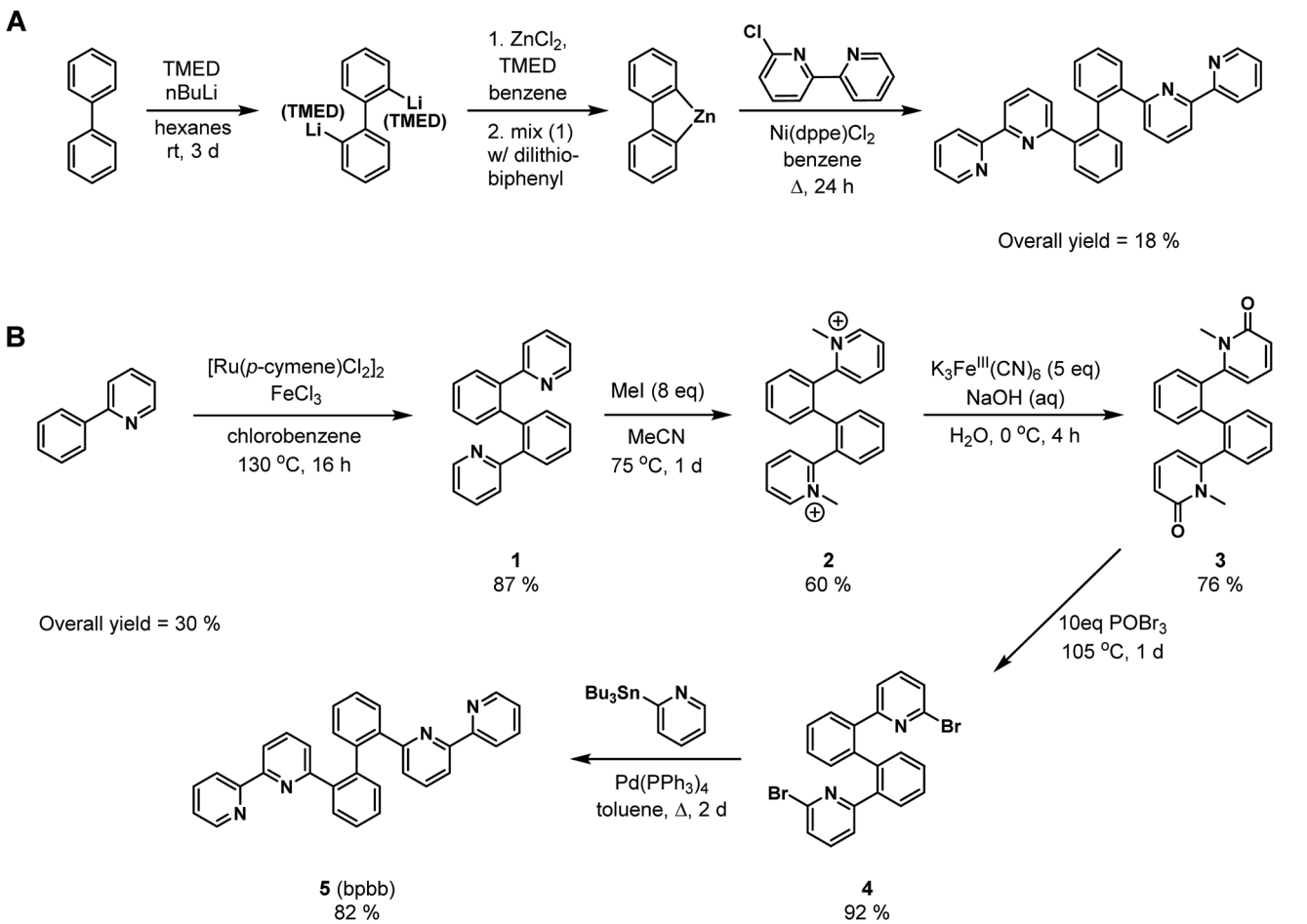

Fig. 1 Synthesis of 2,2′-di([2,2′-bipyridin]-6-yl)-1,1′-biphenyl, **5**. (A) Published route. (B) New route to tetradentate polypyridine ligand.

room temperature overnight. Crystals were readily obtained from concentrated acetonitrile solutions by slow diethyl ether diffusion to give pure complexes in ~90% yield. The complexes are not sensitive to air and moisture.

X-ray crystallography

Solid-state structures were obtained by X-ray crystallography as shown in Fig. 2. The complexes all crystallize in the same space group ($P\bar{1}$) with similar unit cell parameters as presented in Table 1, along with details of data collection. The biphenyl bis(bipyridine) ligand **5** (also abbreviated bpbb) is tetradentate in each complex with its metal–nitrogen bond distances ranging from 1.981 to 2.275 Å (Table 2). From Mn(II) to Ni(II) across the series, distorted octahedral complexes are observed. The metal–ligand bond distances found in **5-Mn**, **5-Fe**, and **5-Co** are consistent with high-spin electronic states.[23] Crystal structures of Cu(I) and Cu(II) complexes with **5** were previously reported;[2] selected bond distances of the Cu(II) complex are also included in Table 2 for comparison with the M(II) complexes reported here. To clarify the coordination configuration of each metal center, coordination polyhedra of the central transition metal atoms were also derived from the crystal structure of each complex as shown in Fig. 2.

The Cu(II) and Zn(II) compounds are five-coordinate species. Using the geometric parameter τ introduced by Addison, Reedijk, and coworkers for five-coordinate structures, the degree of distortion from ideal geometries of square pyramidal and trigonal bipyramidal can be indexed.[24] A value of 1 is obtained for a perfect trigonal bipyramidal geometry while τ is zero for an ideal square pyramidal geometry.[24] Both five-coordinate compounds possess strongly distorted trigonal bipyramidal geometries as indicated by τ = 0.72 for **5-Cu′** and 0.60 for **5-Zn**.

Ligated acetonitrile and an oxyanion complete the primary coordination sphere of the 6-coordinate Mn, Fe, Co, and Ni complexes. Analogous to observations reported of first-row metals supported by a pentadentate polypyridyl ligand,[23] M–N bond distances involving **5** decrease from left to right across the row in the octahedral complexes as expected from the periodic trend for effective ionic radii.[25] This trend is shown graphically in Fig. 3. It is worth noting that the dihedral angle of the biphenyl backbone also decreases as the size of the metal ion becomes smaller in the 6-coordinate complexes. Although composed

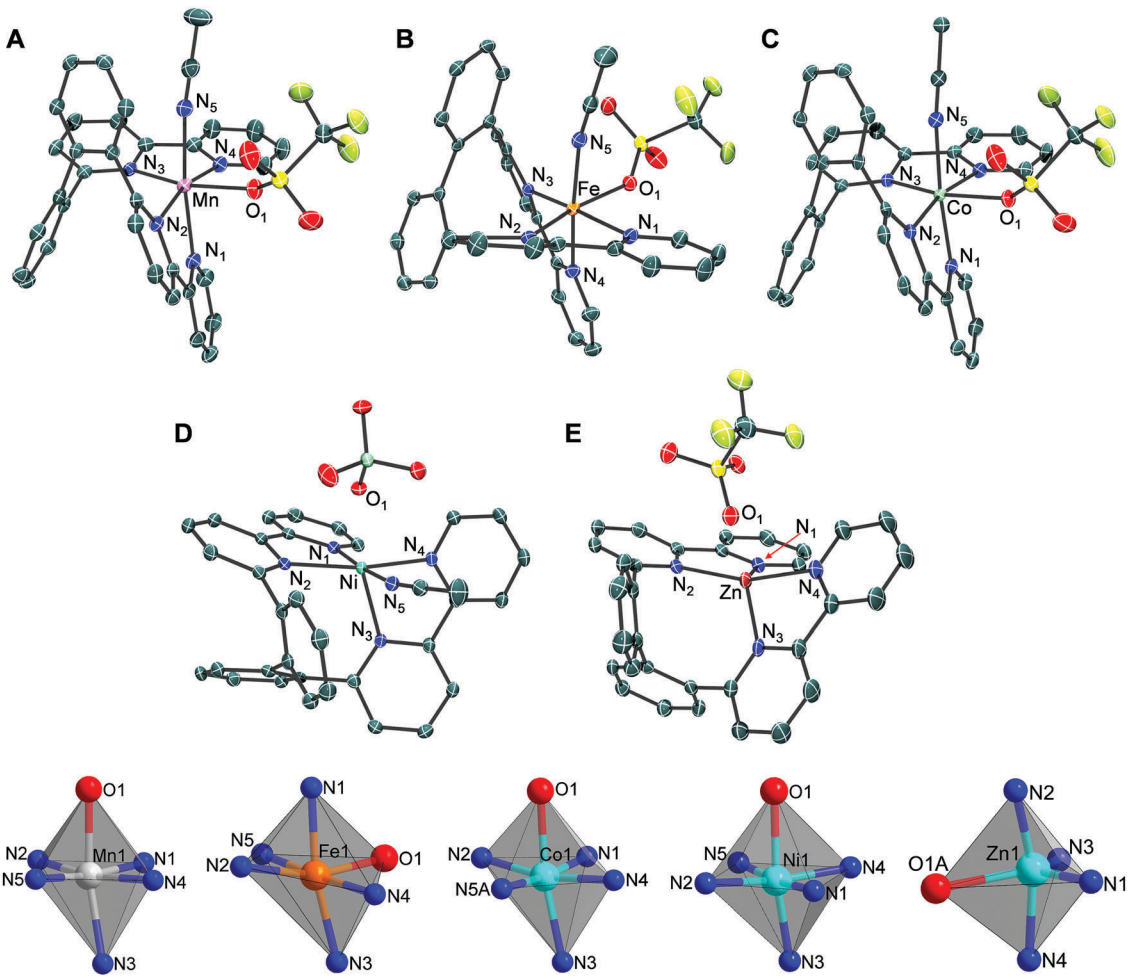

Fig. 2 ORTEP diagrams of cations in **5-Mn** (A), **5-Fe** (B), **5-Co** (C), **5-Ni** (D) and **5-Zn** (E) with thermal ellipsoids rendered at the 50% probability level. Hydrogen atoms have been omitted for clarity. (bottom) Coordination polyhedra constructed from the donor atoms that constitute the immediate coordination sphere around each transition metal ion.

Table 1 Crystallographic data for structures of first-row transition metal complexes supported by **5**

	5-Mn	**5-Fe**	**5-Co**	**5-Ni**	**5-Zn**
Formula	$C_{38}H_{30}F_6MnN_5O_{6.5}S_2$	$C_{38}H_{30}F_6FeN_5O_{6.5}S_2$	$C_{38}H_{30}CoF_6N_5O_{6.5}S_2$	$C_{36}H_{28}Cl_2N_6NiO_8$	$C_{34}H_{22}F_6N_4O_6S_2Zn$
Formula weight	893.73	894.64	897.72	802.25	826.04
Irradiation λ (Å)	0.71073	0.71073	0.71073	0.71073	0.71073
Temperature (K)	100(2)	100(2)	100(2)	100(2)	100(2)
Crystal system	Triclinic	Triclinic	Triclinic	Triclinic	Triclinic
Space group	$P\bar{1}$	$P\bar{1}$	$P\bar{1}$	$P\bar{1}$	$P\bar{1}$
a (Å)	9.2068(3)	9.1892(2)	9.1905(5)	8.8345(3)	9.014(5)
b (Å)	13.8551(5)	13.9385(3)	13.9412(9)	13.4052(4)	13.854(5)
c (Å)	15.2249(5)	15.1654(3)	15.1233(9)	14.4981(5)	14.960(5)
α (°)	85.908(2)	86.1230(10)	86.292(2)	88.5640(10)	86.650(5)
β (°)	84.775(2)	84.0350(10)	83.904(3)	89.0040(10)	87.807(5)
γ (°)	81.762(2)	81.0590(10)	80.749(3)	88.179(2)	80.338(5)
V (Å^3)	1910.73(11)	1905.83(7)	1899.4(2)	1715.34(10)	1837.8(14)
Z	2	2	2	2	2
ρ_{calc} (g cm^{-3})	1.553	1.559	1.570	1.553	1.493
μ (mm^{-1})	0.540	0.591	0.647	0.785	0.861
F(000)	912	914	916	824	886
Crystal size (mm^3)	0.15 × 0.20 × 0.30	0.18 × 0.20 × 0.22	0.10 × 0.10 × 0.30	0.18 × 0.23 × 0.24	0.14 × 0.21 × 0.23
Theta range for collection (°)	1.345 to 24.406	1.35 to 25.36	1.356 to 25.458	1.52 to 25.50	1.36 to 25.38
Index ranges	$-9 \le h \le 10$ $-16 \le k \le 16$ $-17 \le l \le 16$	$-11 \le h \le 11$ $-16 \le k \le 16$ $-18 \le l \le 18$	$-11 \le h \le 11$ $-16 \le k \le 16$ $-18 \le l \le 18$	$-10 \le h \le 10$ $-16 \le k \le 16$ $-17 \le l \le 17$	$-10 \le h \le 10$ $-16 \le k \le 16$ $-17 \le l \le 18$
Reflctns collected	22 804	49 150	27 618	38 473	39 220
Ind. reflctns (R_{int})	5955 (0.0177)	6873 (0.0204)	6681 (0.0272)	6238 (0.0316)	6323 (0.0171)
Data/restr./params	5955/33/554	6873/2/550	6681/108/584	6238/0/480	6323/796/622
Final R indices [$I > 2\sigma(I)$]	R_1 = 0.0371, wR_2 = 0.0861	R_1 = 0.0270, wR_2 = 0.0730	R_1 = 0.0577, wR_2 = 0.1431	R_1 = 0.0248, wR_2 = 0.0682	R_1 = 0.0414, wR_2 = 0.1075
R indices (all data)	R_1 = 0.0417, wR_2 = 0.0897	R_1 = 0.0288, wR_2 = 0.0745	R_1 = 0.0641, wR_2 = 0.1464	R_1 = 0.0252, wR_2 = 0.0685	R_1 = 0.0445, wR_2 = 0.1100
GOF	1.090	0.949	1.159	1.029	1.131
Largest diff. peak and hole (e Å^{-3})	0.728 and −0.348	0.559 and −0.352	1.012 and −0.395	0.327 and −0.440	1.169 and −0.783

Table 2 Selected bond distances of first-row metal complexes supported by **5**

	Coordination environment[a]					
Bond distance	**5-Mn**	**5-Fe**	**5-Co**	**5-Ni**	**5-Cu′**[b]	**5-Zn**
M–N_1	2.238(2)	2.1748(13)	2.096(4)	2.0406(13)	1.981	2.060(2)
M–N_2	2.235(2)	2.2081(13)	2.157(4)	2.1366(13)	2.205	2.112(2)
M–N_3	2.275(2)	2.1967(13)	2.172(4)	2.1339(12)	2.037	2.086(2)
M–N_4	2.238(2)	2.1495(13)	2.131(4)	2.0622(13)	2.060	2.091(2)
M–N_{avg}	2.247	2.182	2.139	2.093	2.071	2.087
M–L	2.227(2) L = MeCN	2.1609(14) L = MeCN	2.134(8) L = MeCN	2.0585(14) L = MeCN	2.305 L = Cl	—
M–O[c]	2.2001(17)	2.1491(11)	2.181(3)	2.2208(11)	—	2.21(2)
Dihedral angle[d]	121.4°	118.9°	117.0°	108.4°	119.4°	109.4°

[a] All bond distances are reported in Angstroms (Å). [b] From ref. 2 where **5-Cu′** is [Cu(bpbb)Cl](ClO$_4$)·MeCN. [c] Bound oxygen donor of coordinated oxyanion, triflate or perchlorate. [d] Dihedral angle of biphenyl backbone.

entirely of interconnected aromatic rings, the global flexibility in torsion angles enables **5** to accommodate metals of different size.

A comparison of bond distances of the pyridine donors adjacent to the biphenyl (M–N_2, M–N_3) *versus* the distal pyridine donors of each bipyridine unit (M–N_1, M–N_4) reveals that, in general, the former have longer bond distances than the latter, indicating that the interior donors are more constrained by the demands of the ligand and bind less strongly to the metal center. The impact of the biphenyl bridge on the bipyridine (bpy) coordination chemistry of these complexes was assessed further by comparison to relevant metal bis(bipyridine) complexes from the literature. Tables S1–S6 of the ESI† are grouped by each metal from Mn(II) to Zn(II) and contain the metal–ligand bond distances of selected compounds, their associated references, and CCDC deposition numbers.

As typically found for d^5 manganese compounds, **5-Mn** and the Mn(II) complexes listed in Table S1 (ESI†) have bond distances that are consistent with high-spin electronic states. Interestingly, the average Mn–N (bpy) bond distance observed in **5-Mn** is shorter (by ∼0.01 to 0.02 Å) than that of the related Mn(II) ions comprised of two unsubstituted 2,2′-bipyridine ligands and carrying an overall charge of +1.[26–30] This result is in contrast to the remaining complexes supported by ligand **5** which tend to have longer M–N (bpy) bond distances relative to

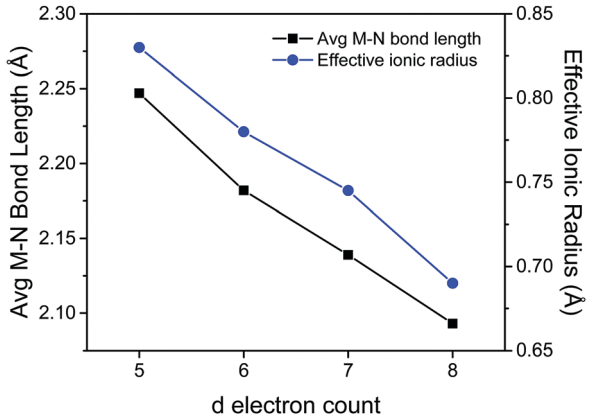

Fig. 3 Plot of average metal–nitrogen bond length (Å) involving **5** and the effective ionic radius (Å) as a function of d electron count for the six-coordinate metals (**5-Mn**, **5-Fe**, **5-Co**, and **5-Ni**).

the unsubstituted 2,2′-bipyridine donors. Given the collective preference for the high-spin electron configuration, the relatively shorter M–N (bpy) bond distances observed in **5-Mn** suggests that **5** is suitably matched to Mn(II), which has the largest effective ionic radius of the M(II) ions investigated here, allowing stronger metal–ligand bonding interactions.

Only a limited comparison of **5-Fe** was possible with iron(II) bis(bipyridine) complexes.[31,32] Indeed, $[Fe(bpy)_2L_2]^{n+}$ complexes (where L is a labile monodentate ligand) are very rare due to formation of the thermodynamically favored d^6 spin-paired $[Fe(bpy)_3]^{2+}$ complex.[31,32] However, crystal structures with mononuclear $Fe(bpy)_2$ cores were found with anionic donors Cl^-, CN^-, and NCS^- completing the octahedral coordination spheres (Table S2, ESI†).[33–35] Despite the overall +1 positive charge of **5-Fe**, its average Fe–N (bpy) bond distance is longer than that of the neutral compounds $Fe(bpy)_2Cl_2$,[33] $Fe(bpy)_2(CN)_2$,[34] and $Fe(bpy)_2(NCS)_2$.[35] The longer bond lengths observed with **5-Fe** are consistent with a high-spin electronic state and highlight the weaker ligand field afforded by the rigid biphenyl-based ligand **5**. In addition, a strong temperature dependence was reported for $Fe(bpy)_2(NCS)_2$ in solid-state structures determined at 110 and 298 K, which have average Fe–N (bpy) bond lengths of 1.967 and 2.174 Å, respectively, indicating a change from low-spin (110 K) to high-spin (298 K).[35] This behavior is not observed with **5-Fe**, which has an average Fe–N (bpy) bond length of 2.183 Å in the solid-state at 100 K.

Crystal structures of selected cobalt(II) complexes were also compared with **5-Co** (Table S3, ESI†). Again, the average cobalt–pyridine bond distance of **5-Co** (2.139 Å) was found to be longer relative to $Co(bpy)_2$ ions bearing an anionic donor,[36,37] reflecting the structural constraints of the tetradentate ligand. Nearly equivalent average Co–N (bpy) bond distances were observed between **5-Co** and neutral $Co(bpy)_2Cl_2$ (2.142 Å),[38] which are ~0.08 Å longer than that of $[Co(bpy)_2(OH_2)_2]^{2+}$ as expected on the basis of overall charge.[39] Similar observations were made for **5-Ni** with respect to relevant octahedral nickel(II) compounds featuring two unsubstituted 2,2′-bipyridine donors.[40–44] As summarized in Table S4 (ESI†), average Ni–N (bpy) bond lengths ranged from 2.059 Å for $[Ni(bpy)_2(OH_2)(ONO_2)]^+$ to 2.091 Å for $Ni(bpy)_2Cl_2$, while the average nickel–pyridine bond distance for **5-Ni** is 2.094 Å.

Next, the five-coordinate copper(II) and zinc(II) complexes were compared to related bis(bipyridine) compounds. Copper compound (**5-Cu′**) bearing **5** and a chloro ligand has an average Cu–N (bpy) bond distance of 2.071 Å.[2] Consistent with the bridled coordination of **5** noted above, this average bond distance is longer by ~0.02 to 0.03 Å relative to the average Cu–N (bpy) bond distances found in crystal structures of several $[Cu(bpy)_2Cl]^+$ salts (Table S5, ESI†).[45–47] In the same vein, **5-Zn**, ligated by the biphenyl-based polypyridine and a triflato donor, has an average zinc–pyridine bond distance of 2.088 Å which is longer than that of both $[Zn(bpy)_2Cl]^+$ and $[Zn(bpy)_2(OH_2)]^{2+}$ (Table S6, ESI†).[48,49] Together these results indicate that the biphenyl bridge restrains bipyridine coordination to mid-to-late first-row metal centers.

Electrochemistry

Cyclic voltammetry was conducted in anhydrous acetonitrile with the title compounds (Fig. 4). Multiple redox processes were observed in the cyclic voltammograms (CVs) over a wide potential range (>3 V); $E_{1/2}$ values and peak potentials for the irreversible redox features are summarized in Table 3. All potentials are reported in volts *versus* the ferrocenium/ferrocene couple (V *vs.* $Fc^{+/0}$). Irreversible to quasi-reversible metal-based oxidations occur at 0.67 V (**5-Mn**), 0.95 V (**5-Fe**), 0.74 V (**5-Co**), each of which is a $M^{III/II}$ process, and at 0.09 V (**5-Cu**) which we assign to a $Cu^{II/I}$ couple. Similar oxidations were not observed with **5-Ni** and **5-Zn**. As expected, **5-Zn** is electrochemically silent at potentials positive of −1.4 V. The zinc complex, featuring a redox-inactive metal center, is useful in identifying ligand-based redox events and has redox couples at −1.47, −1.58, and −2.17, followed by an irreversible reduction at −2.45 V. Consistent with previous observations,[2] **5-Cu** exhibits two ligand-based reductions at −2.07 and −2.26 V. Upon scanning positive, a sharp return oxidation is observed at −0.71 V, which is likely due to adsorption on the electrode surface given the reversible behavior

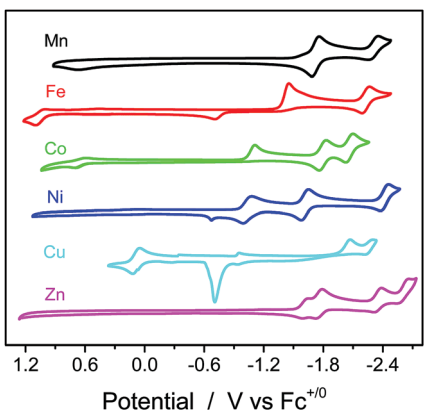

Fig. 4 CVs of **5-Mn**, **5-Fe**, **5-Co**, **5-Ni**, **5-Cu**, and **5-Zn** (at 1 mM concentrations) in anhydrous acetonitrile/0.1 M Bu_4NPF_6 solutions using a glassy carbon disk electrode, ν = 100 mV s^{-1}.

Table 3 Redox properties of each complex in acetonitrile with 0.1 M Bu_4NPF_6, ν = 100 mV s^{-1}

Complex	Redox potentials (V *vs.* $Fc^{+/0}$)				
5-Mn	0.67[b]	−1.71	−2.30	—	—
5-Fe	0.95[b]	−1.53[c]	−2.30	—	—
5-Co	0.74	−1.03[c]	−1.69	−1.96	—
5-Ni	—	−1.03	−1.57	−2.38	—
5-Cu[a]	0.09	−0.71[b]	−2.07[c]	−2.26[c]	—
5-Zn	—	−1.47	−1.58	−2.17	−2.45[c]

[a] **5-Cu** is $[Cu(bpbb)](ClO_4)_2 \cdot MeCN \cdot H_2O$ as reported in ref. 2. [b] Irreversible ($E_{p,a}$). [c] Irreversible ($E_{p,c}$).

previously reported with this compound in acetonitrile using Bu_4NClO_4 as the supporting electrolyte.[2] Compound **5-Ni** has three reversible redox processes at −1.03, −1.57, and −2.38 V that are tentatively assigned to $Ni^{II/I}$ and $Ni^{I/0}$ metal-based couples followed by a ligand-localized reduction, respectively. For **5-Co**, an irreversible feature at −1.03 V is assigned to a $Co^{II/I}$ reduction with two reversible couples at −1.69 and −1.96 V occurring that are likely ligand centered. Similarities in the CVs of **5-Fe** and **5-Mn** are apparent. Each complex has a two-electron reduction at −1.53 V (**5-Fe**) and −1.71 V (**5-Mn**), which are at similar potentials to the initial overlapping one-electron reductions of **5-Zn**. On this basis, we assign these events as ligand-based reductions and the most negative waves to $M^{II/I}$ couples.

To assess the influence of the biphenyl backbone on redox potentials, the electrochemical data summarized in Table 3 was compared to related first-row metal bis- and tris-bipyridine complexes (Table S7, ESI†).[36,50–58] Here, bipyridine-based reductions were generally found from approximately −1.3 to −2.3 V *vs.* $Fc^{+/0}$. Interestingly, metal-based redox couples of the complexes supported by **5** are typically more positive than those of the corresponding $[M(bpy)_3]^{2+}$ complexes, with the exception of **5-Mn**. The processes assigned to the $Fe^{III/II}$ couples of **5-Fe** and $[Fe(bpy)_3]^{2+}$ occur at 0.95 and 0.69 V, respectively,[51] whereas the $Mn^{III/II}$ couples of **5-Mn** and $[Mn(bpy)_3]^{2+}$ appear at 0.67 and 0.93 V, respectively.[50] Likewise, the $Cu^{II/I}$ couple of **5-Cu** is observed at 0.09 V, or nearly 600 mV more positive than for $[Cu(bpy)_3]^{2+}$.[57] These metal-based redox potentials are consistent with the observed metal–pyridine bond distances. Stronger Lewis acid–base bonding interactions are observed in **5-Mn** compared to related Mn(II) compounds, which results in greater electron density at the metal and a cathodic shift of the $Mn^{III/II}$ couple. However, weaker bonds to each metal center are present for the remaining compounds relative to their $[M(bpy)_3]^{2+}$ counterparts, which give rise to anodic shifts in the metal-based redox couples.

UV-visible spectroscopy

UV-visible spectra of the compounds in acetonitrile are shown in Fig. 5; associated absorption maxima and molar extinction coefficients are presented in Table 4. An intense π-to-π* transition at around 310 nm (~22 000 M^{-1} cm^{-1}) is observed for all five metal complexes. Given the high-spin electronic states afforded by the constrained biphenyl bis(bipyridine) ligand, the complexes have little-to-no absorbance in the visible region. The iron complex **5-Fe** has a weak absorption band at 410 nm (660 M^{-1} cm^{-1}) that is ascribed to a metal-to-ligand charge transfer (MLCT) transition. Broad, low-intensity bands assigned to Laporte-forbidden d–d transitions are observed at 815 nm (**5-Fe**), 482 nm (**5-Co**), and 550 and 923 nm (**5-Ni**) consistent with the solid-state structures and distorted octahedral compounds in solution. Likewise, two broad bands at 677 and 960 nm are characteristic of **5-Cu**.

Magnetism

The Evans method was used to determine solution magnetic susceptibilities across the series as summarized in Table 4. The experimental magnetic moments are close to the theoretical values expected for high-spin electronic states and/or the d^n electron configuration of each M(II) ion, for example, as in d^9 Cu(II) which will have one unpaired electron regardless of geometry or spin state. The deviation in the measured value (4.5 μ_B) for **5-Co** from the anticipated theoretical spin-only magnetic moment (3.87 μ_B) is common of cobalt complexes, including a previously reported high-spin Co(II) polypyridyl complex,[23] and indicative of an overall magnetic moment with significant orbital contribution.[59]

Intrigued by the work of Petzold and coworkers who have developed iron(II) compounds supported by hexadentate and

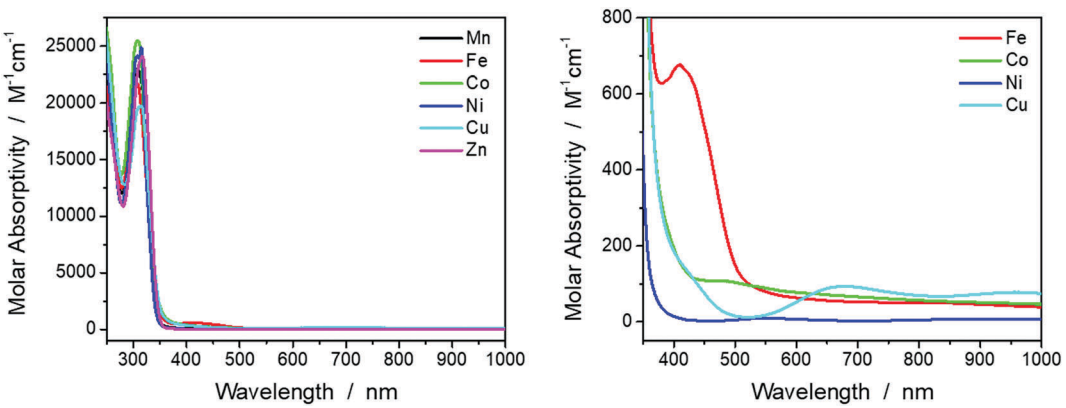

Fig. 5 UV-visible spectra of Mn(II), Fe(II), Co(II), Ni(II), Cu(II), and Zn(II) complexes with ligand **5** in acetonitrile.

Table 4 UV-vis spectral properties and solution magnetic susceptibility of metal complexes bearing **5**

5-Mn	5-Fe	5-Co	5-Ni	5-Cu	5-Zn
UV-Vis					
308 (22 827)	307 (22 100) 410 (660) 815 (50)	308 (25 100) 482 (110)	307 (23 800) 550 (10) 923 (10)	315 (19 000) 677 (100) 960 (100)	317 (23 500)
μ_{eff} at 298 K (μ_B)					
5.9	5.2	4.5	2.7	1.5	—

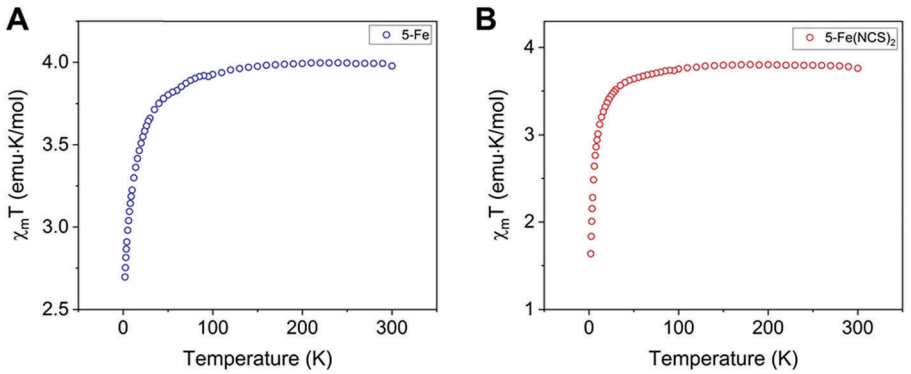

Fig. 6 Temperature dependence of $\chi_m T$ for **5-Fe** (A) and **5-Fe(NCS)$_2$** (B).

dinucleating biphenyl-based N-donor ligands that exhibit spin crossover behavior,[5] we prepared a bis(thiocyanato) derivative **5-Fe(NCS)$_2$**, in addition to **5-Fe**. Their temperature-dependent magnetic behavior was investigated by solid-state SQUID magnetometry. For compounds **5-Fe** and **5-Fe(NCS)$_2$**, the plots of DC susceptibility *vs.* temperature exhibited room temperature $\chi_m T$ values of 3.98 emu K mol^{-1} and 3.76 emu K mol^{-1} (indicative of electron *g*-factors greater than 2.00), which steadily decreased to final $\chi_m T$ values of 2.70 emu K mol^{-1} and 1.64 emu K mol^{-1} respectively (Fig. 6). Room temperature $\chi_m T$ values for high-spin Fe(II) complexes are generally in the range of 3–3.5,[60] but higher values have been reported as well.[61] This steady decrease in $\chi_m T$ can be attributed to zero-field splitting in the complexes and/or thermal depopulation of excited electronic states. Spin crossover behavior was not observed as the compounds maintained high-spin electron configurations over the entire temperature range, as indicated by the absence of a precipitous drop of the $\chi_m T$ values at lower temperatures.

Conclusions

In closing, we report an improved synthesis of a rigid polyaromatic N_4-donor ligand and have greatly expanded its known coordination chemistry. Structural, electrochemical, spectroscopic, and magnetic properties of a series of mid-to-late first-row transition metal complexes supported by the tetradentate polypyridine scaffold have been investigated. From X-ray crystallography, the ligand field around each metal ion is noticeably constrained by the limited flexibility (confined to rotation about the single bonds connecting each aromatic unit) afforded by the biphenyl backbone. High spin electronic states, based in part on the metal–ligand bond lengths, and distorted octahedral geometries are observed for the Mn(II), Fe(II), and Co(II) complexes. Distorted trigonal bipyramidal geometries are found in solid-state structures of the Cu(II) and Zn(II) derivatives. Indeed, the optical spectra, solution magnetic susceptibility measurements, and temperature-dependent SQUID magnetometry data are consistent in both the solid-state and solution analyses, confirming the structural integrity of the dissolved complexes remains intact.

Notably, **5-Fe** represents a rare example of an iron bis(bipyridine) complex possessing two labile monodentate ligands. Synthetic routes to $[Fe(bpy)_2L_2]^{n+}$ complexes are elusive due to the favored formation of the tris(bpy) complex, which is a consequence of a change from high spin to low spin between $[Fe(bpy)_2L_2]^{n+}$ to the more stable spin-paired $[Fe(bpy)_3]^{2+}$ ion.[31,32] In addition to steric considerations, we hypothesize that the biphenyl-linked bis(bipyridine) ligand may prevent this spin change and negate the thermodynamic driving force that would otherwise favor the tris(bpy) derivative. Spin crossover behavior was not observed in the iron(II) compounds **5-Fe** and **5-Fe(NCS)$_2$**. These results indicate that **5** weakens the ligand field strength around iron and, due to its limited flexibility, may be less accommodating to the changes in metal–ligand bond distances that accompany a spin transition from high-to-low.

Conflicts of interest

There are no conflicts to declare.

Acknowledgements

Acknowledgment is made to the donors of The American Chemical Society Petroleum Research Fund for support of this

research (58707-DNI3). We also acknowledge seed grant funding from the National Science Foundation (OIA-1539035) and start-up support from the University of Mississippi.

References

1 (*a*) T. J. Collins, *Acc. Chem. Res.*, 1994, **27**, 279–285; (*b*) P. Comba, *Coord. Chem. Rev.*, 1999, **182**, 343–371; (*c*) R. D. Hancock, *Chem. Soc. Rev.*, 2013, **42**, 1500–1524.
2 E. Müller, C. Piguet, G. Bernardinelli and A. F. Williams, *Inorg. Chem.*, 1988, **27**, 849–855.
3 (*a*) O. P. Anderson, J. Becher, H. Frydendahl, L. F. Taylor and H. Toftlund, *J. Chem. Soc., Chem. Commun.*, 1986, 699–701; (*b*) S. Knapp, T. P. Keenan, X. Zhang, R. Fikar, J. A. Potenza and H. J. Schugar, *J. Am. Chem. Soc.*, 1990, **112**, 3452–3464; (*c*) E. Müller, G. Bernardinelli and J. Reedijk, *Inorg. Chem.*, 1996, **35**, 1952–1957; (*d*) M. R. Malachowski, M. Adams, N. Elia, A. L. Rheingold and R. S. Kelly, *J. Chem. Soc., Dalton Trans.*, 1999, 2177–2182.
4 (*a*) M. Réglier, C. Jorand and B. Waegell, *J. Chem. Soc., Chem. Commun.*, 1990, 1752–1755; (*b*) M. R. Malachowski, A. S. Kasto, M. E. Adams, A. L. Rheingold, L. N. Zakharov, L. D. Margerum and M. Greaney, *Polyhedron*, 2009, **28**, 393–397.
5 (*a*) H. Petzold and S. Heider, *Eur. J. Inorg. Chem.*, 2011, 1249–1254; (*b*) S. Heider, H. Petzold and G. Teucher, *Eur. J. Inorg. Chem.*, 2013, 2382–2388.
6 (*a*) M. Kettunen, C. Vedder, F. Schaper, M. Leskelä, I. Mutikainen and H.-H. Brintzinger, *Organometallics*, 2004, **23**, 3800–3807; (*b*) C. Vedder, F. Schaper, H.-H. Brintzinger, M. Kettunen, S. Babik and G. Fink, *Eur. J. Inorg. Chem.*, 2005, 1071–1080; (*c*) G. J. P. Britovsek, J. England and A. J. P. White, *Dalton Trans.*, 2006, 1399–1408; (*d*) T. Chen, X.-G. Liu and M. Shi, *Tetrahedron*, 2007, **63**, 4874–4880.
7 M. A. Halcrow, *Polyhedron*, 2007, **26**, 3523–3576.
8 S. O. Schmidt, S. Kisslinger, C. Würtele, S. Bonnet, S. Schindler and F. Tuczek, *Z. Anorg. Allg. Chem.*, 2013, **639**, 2774–2778.
9 P. Gütlich, A. B. Gaspar and Y. Garcia, *Beilstein J. Org. Chem.*, 2013, **9**, 342–391.
10 (*a*) A. Bousseksou, G. Molnár, L. Salmon and W. Nicolazzi, *Chem. Soc. Rev.*, 2011, **40**, 3313–3335; (*b*) S. Brooker, *Chem. Soc. Rev.*, 2015, **44**, 2880–2892; (*c*) M. A. Halcrow, *Crystals*, 2016, **6**, 58.
11 E. C. Constable, G. Baum, E. Bill, R. Dyson, R. van Eldik, D. Fenske, S. Kaderli, D. Morris, A. Neubrand, M. Neuburger, D. R. Smith, K. Wieghardt, M. Zehnder and A. D. Zuberbühler, *Chem. – Eur. J.*, 1999, **5**, 498–508.
12 E. D. McKenzie, *Coord. Chem. Rev.*, 1971, **6**, 187–216.
13 D. Onggo and H. A. Goodwin, *Aust. J. Chem.*, 1991, **44**, 1539–1551.
14 (*a*) L. Chen, A. Khadivi, M. Singh and J. W. Jurss, *Inorg. Chem. Front.*, 2017, **4**, 1649–1653; (*b*) X. Su, K. M. McCardle, J. A. Panetier and J. W. Jurss, *Chem. Commun.*, 2018, **54**, 3351–3354; (*c*) W. Yang, S. Sinha Roy, W. C. Pitts, R. Nelson, F. R. Fronczek and J. W. Jurss, *Inorg. Chem.*, 2018, **57**, 9564–9575.
15 (*a*) D. F. Evans, *J. Chem. Soc.*, 1959, 2003–2005; (*b*) G. A. Bain and J. F. Berry, *J. Chem. Educ.*, 2008, **85**, 532–536.
16 APEX2, v. 2009, Bruker Analytical X-Ray Systems, Inc, Madison, WI, 2009.
17 G. M. Sheldrick, *SADABS, Version 2.03*, Bruker Analytical X-ray Systems, Inc, Madison, WI, 2000.
18 (*a*) G. M. Sheldrick, *Acta Crystallogr., Sect. A: Found. Crystallogr.*, 1990, **46**, 467–473; (*b*) G. M. Sheldrick, *Acta Crystallogr., Sect. A: Found. Crystallogr.*, 2008, **64**, 112–122; (*c*) G. M. Sheldrick, *SHELXL-2014/7: Program for crystal structure determination*, University of Göttingen, Göttingen, Germany, 2014.
19 (*a*) A. L. Spek, *PLATON – A Multipurpose Crystallographic Tool*, Utrecht University, Utrecht, The Netherlands, 2007; (*b*) A. L. Spek, PLATON SQUEEZE: A tool for the calculation of the disordered solvent contribution to the calculated structure factors, *Acta Crystallogr., Sect. C: Struct. Chem.*, 2015, **71**, 9–18.
20 H. Putz and K. Bradenburg, *Diamond – Crystal and Molecular Structure Visualization*, Crystal Impact: GbR, Kreuzherrenstr., 102, 53227 Bonn, Germany, http://www.crystalimpact.com/diamond.
21 X. Guo, G. Deng and C.-J. Li, *Adv. Synth. Catal.*, 2009, **351**, 2071–2074.
22 M. Böttger, B. Wiegmann, S. Schaumburg, P. G. Jones, W. Kowalsky and H.-H. Johannes, *Beilstein J. Org. Chem.*, 2012, **8**, 1037–1047.
23 R. J. M. Klein Gebbink, R. T. Jonas, C. R. Goldsmith and T. D. P. Stack, *Inorg. Chem.*, 2002, **41**, 4633–4641.
24 A. W. Addison, T. N. Rao, J. Reedijk, J. van Rijn and G. C. Verschoor, *J. Chem. Soc., Dalton Trans.*, 1984, 1349–1356.
25 R. D. Shannon, *Acta Crystallogr., Sect. A: Cryst. Phys., Diffr., Theor. Gen. Crystallogr.*, 1976, **32**, 751–767.
26 N. Palanisami and R. Murugavel, *Inorg. Chim. Acta*, 2011, **365**, 430–438.
27 K. B. Dillon, C. Bilton, J. A. K. Howard, V. J. Hoy, R. M. K. Deng and D. T. Sethatho, *Acta Crystallogr., Sect. C: Cryst. Struct. Commun.*, 1999, **55**, 330–332.
28 M. Shao, Z.-X. Miao and M.-X. Li, *Acta Crystallogr., Sect. E: Struct. Rep. Online*, 2006, **62**, m2575–m2577.
29 G. Fernández, M. Corbella, M. Alfonso, H. Stoeckli-Evans and I. Castro, *Inorg. Chem.*, 2004, **43**, 6684–6698.
30 X.-M. Chen, K.-L. Shi, T. C. W. Mak and B.-S. Luo, *Acta Crystallogr., Sect. C: Cryst. Struct. Commun.*, 1995, **51**, 358–361.
31 H. Irving and D. H. Mellor, *J. Chem. Soc.*, 1962, 5222–5237.
32 M.-N. Collomb, A. Deronzier, K. Gorgy and J.-C. Leprêtre, *New J. Chem.*, 2000, **24**, 455–461.
33 S. Parsons, R. Winpenny and P. A. Wood, *CCDC 248214: Experimental Crystal Structure Determination*, 2014, DOI: 10.5517/cc8b8xr.
34 Y. Wang, X. Ma, S. Hu, Y. Wen, Z. Xue, X. Zhu, X. Zhang, T. Sheng and X. Wu, *Dalton Trans.*, 2014, **43**, 17453–17462.
35 M. Konno and M. Mikami-Kido, *Bull. Chem. Soc. Jpn.*, 1991, **64**, 339–345.
36 S.-P. Luo, L.-Z. Tang and S.-Z. Zhan, *Inorg. Chem. Commun.*, 2017, **86**, 276–280.
37 S. Gao, J.-W. Liu, L.-H. Huo and H. Zhao, *Acta Crystallogr., Sect. E: Struct. Rep. Online*, 2004, **60**, m1202–m1204.

38 K. A. Kumar, M. Amuthaselvi and A. Dayalan, *Acta Crystallogr., Sect. E: Struct. Rep. Online*, 2011, **67**, m468.
39 V. Ciornea, L. Mingalieva, J.-P. Costes, G. Novitchi, I. Filippova, R. T. Galeev, S. Shova, V. K. Voronkova and A. Gulea, *Inorg. Chim. Acta*, 2008, **361**, 1947–1957.
40 B.-S. Zhang, Z.-X. Liu, L.-H. Liu, T. Pan and S.-F. Ye, *Acta Crystallogr., Sect. E: Struct. Rep. Online*, 2009, **65**, m48.
41 M. Garai, D. Dey, H. R. Yadav, A. R. Choudhury, N. Kole and B. Biswas, *Polyhedron*, 2017, **129**, 114–122.
42 D. J. Chesnut, R. C. Haushalter and J. Zubieta, *Inorg. Chim. Acta*, 1999, **292**, 41–51.
43 Y. Rodríguez-Martín, J. González-Platas and C. Ruiz-Pérez, *Acta Crystallogr., Sect. C: Cryst. Struct. Commun.*, 1999, **55**, 1087–1090.
44 B. Hipler, M. Döring, C. Dubs, H. Görls, T. Hübler and E. Uhlig, *Z. Anorg. Allg. Chem.*, 1998, **624**, 1329–1335.
45 M. A. Sharif, M. Tabatabaee, V. Beik and H. R. Khavasi, *CCDC 749881: Experimental Crystal Structure Determination*, 2014, DOI: 10.5517/cct59qz.
46 A. Jayamani, N. Sengottuvelan, S. K. Kang and Y.-I. Kim, *Polyhedron*, 2015, **98**, 203–216.
47 P. Nagle, E. O′Sullivan, B. J. Hathaway and E. Müller, *J. Chem. Soc., Dalton Trans.*, 1990, **0**, 3399–3406.
48 J.-C. Yao, F.-J. Yao, J.-B. Guo, W. Huang and S.-H. Gou, CCDC 271110: Experimental Crystal Structure Determination, 2014, DOI: 10.5517/cc933hz.
49 G. Singh, I. P. S. Kapoor, D. Kumar, U. P. Singh and N. Goel, *Inorg. Chim. Acta*, 2009, **362**, 4091–4098.
50 S. A. Richert, P. K. S. Tsang and D. T. Sawyer, *Inorg. Chem.*, 1989, **28**, 2471–2475.
51 J. P. F. Rebolledo-Chávez, M. Cruz-Ramírez, R. Patakfalvi, F. J. Tenorio Rangel and L. Ortiz-Frade, *Electrochim. Acta*, 2017, **247**, 241–251.
52 M.-N. Collomb, A. Deronzier, K. Gorgy and J.-C. Leprêtre, *New J. Chem.*, 2000, **24**, 455.
53 M. A. W. Lawrence and A. A. Holder, *Inorg. Chim. Acta*, 2016, **441**, 157.
54 R. Prasad and D. B. Scaife, *J. Electroanal. Chem.*, 1977, **84**, 373–386.
55 P. N. Bartlett and V. Eastwick-Field, *Electrochim. Acta*, 1993, **38**, 2515–2523.
56 O. S. Fomina, Y. A. Kislitsyn, V. M. Babaev, I. K. Rizvanov, O. G. Sinyashin, J. W. Heinicke and D. G. Yakhvarov, *Russ. J. Electrochem.*, 2015, **51**, 1069–1078.
57 R. R. Ruminski, *Inorg. Chim. Acta*, 1985, **103**, 159–161.
58 R. J. Crutchley, R. Hynes and E. J. Gabe, *Inorg. Chem.*, 1990, **29**, 4921–4928.
59 F. A. Cotton and G. Wilkinson, *Advanced Inorganic Chemistry*, Wiley-Interscience: New York, 5th edn, 1988.
60 S. Kisslinger, H. Kelm, S. Zheng, A. Beitat, C. Würtele, R. Wortmann, S. Bonnet, S. Herres-Pawlis, H.-J. Krüger and S. Schindler, *Z. Anorg. Allg. Chem.*, 2012, **638**, 2069–2077.
61 A. Kimura and T. Ishida, *Inorganics*, 2017, **5**, 52–63.